Supplemental material

Heymann et al., https://doi.org/10.1083/jcb.201806148

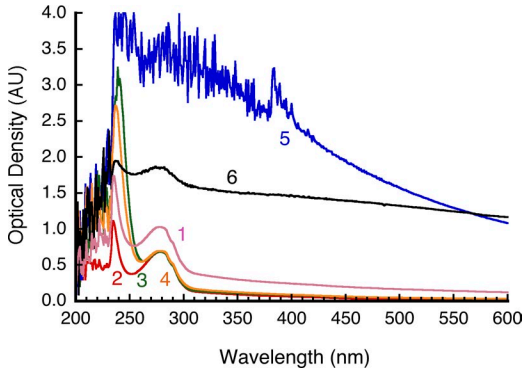

Figure S1. **Assessment of retinoschisin by optical density in different buffers shows massive aggregation in the presence of calcium.** All at a protein concentration of 0.1 mg/ml and pH 7.4. **(1)** 20 mM phosphate, 500 mM NaCl, and 200 mM imidazole (control). **(2)** 20 mM Tris, 500 mM NaCl, and 200 mM imidazole. **(3)** 20 mM phosphate, 700 mM NaCl, and 50 mM EDTA. **(4)** 20 mM phosphate, 100 mM NaCl, and 50 mM EDTA. **(5)** 20 mM Tris, 700 mM NaCl, and 20 mM $CaCl_2$. **(6)** 20 mM Tris, 100 mM NaCl, and 20 mM $CaCl_2$. Data shown from one experiment.

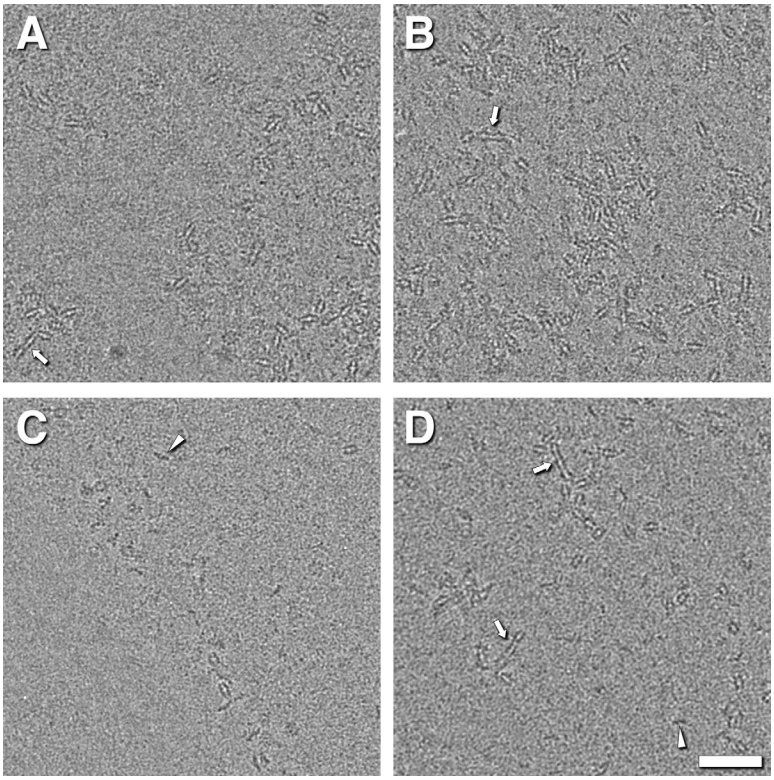

Figure S2. **Cryo-electron micrographs of RS1 under different buffer conditions.** The panels correspond to four of the samples shown in Fig. S1: **(A)** 1, phosphate/imidazole/high salt; **(B)** 2, Tris/imidazole/high salt; **(C)** 3, Tris/EDTA/high salt; and **(D)** 4, Tris/EDTA/low salt. The arrows indicates linear strings of RS1 molecules, and the arrowheads point to single octamer rings. A and B differ only in the buffering compound used and show similar distributions of interactions. In C and D, the presence of EDTA may lead to some dissociation of RS1 into single octamers (arrowheads) or even smaller oligomers. In D, individual molecules, single octamers, and strings of RS1 are apparent, although at a lower concentration. The latter suggests that the strings are able to form at more physiological salt concentrations. Imaged on a JEOL 2200FS operated at 200 kV with a K2 Summit camera.

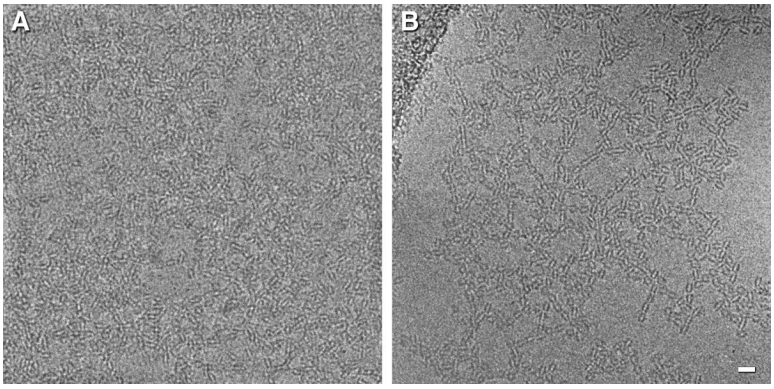

Figure S3. **Cryo-EM of RS1 under string-forming conditions with and without galactose. (A and B)** Micrographs of plunge-frozen RS1 molecules without (A) and with (B) galactose (10 mM final concentration) and in high-salt buffer (20 mM sodium phosphate, 200 mM imidazole, and 500 mM NaCl, pH 7.4). Imaged on a CM200 microscope operated at 120 kV with a CCD camera.

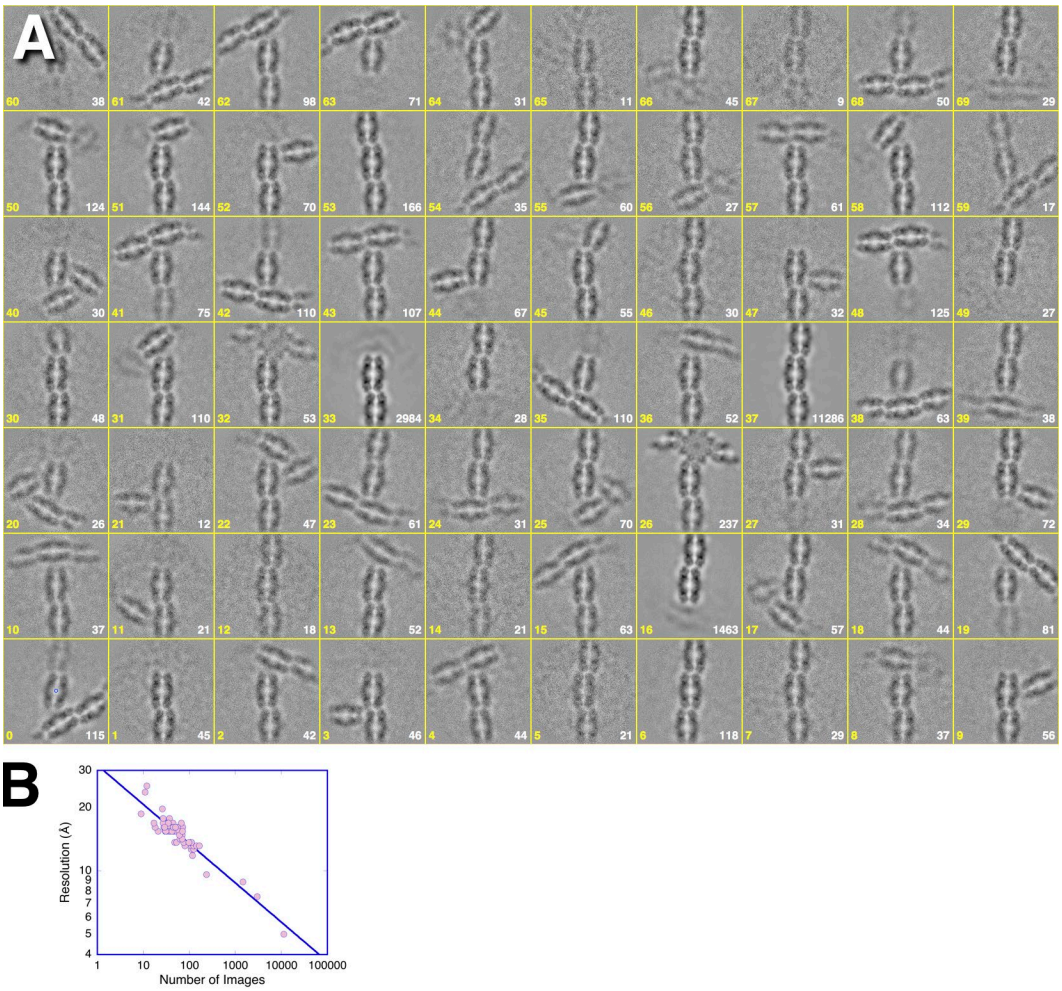

Figure S4. **2D class averages of RS1 in filamentous networks. (A)** The 70 final class averages from the first data set with the white numbers indicate the contributing boxes. The most prevalent class is 37, composed from more than half of the boxes. **(B)** Resolution of the 2D averages shown in A calculated at a spectral signal-to-noise ratio cutoff of 0.5. Several of these class averages are shown in Fig. 2, in some cases after further alignment and centering.

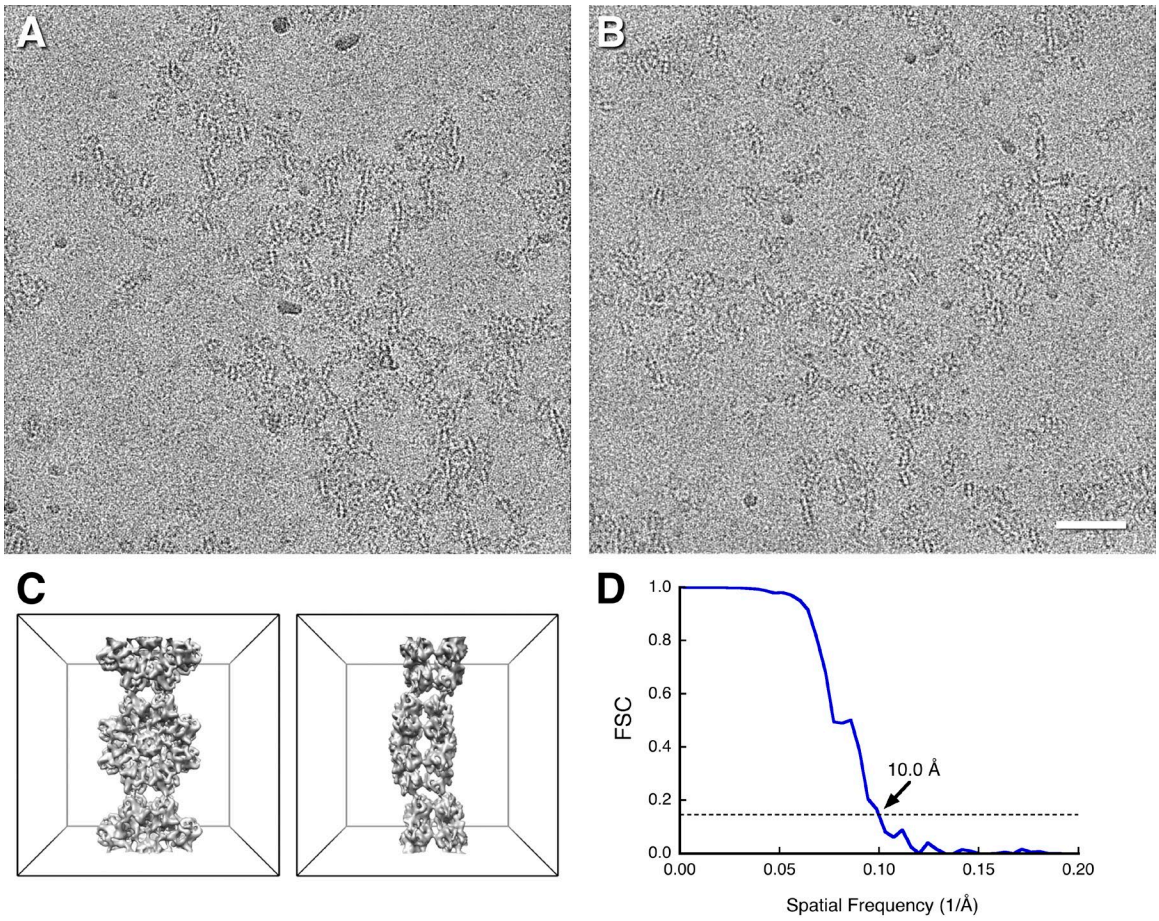

Figure S5. **3D reconstruction of the RS1 linear strand unit cell from micrographs of tilted specimens. (A and B)** Micrographs of RS1 from the second data set taken at a 30° tilt angle to obtain oblique views for 3D reconstruction (conditions as in Fig. S2 with 10 mM galactose). Imaged on a Krios microscope operated at 300 kV with a K2 camera. **(C)** The main string interactions (type I) of the RS1 molecules can be described as a 1D crystal consistent with the space group $P222_1$, with a twofold axis passing through the center of one molecule and a twofold screw axis relating the two molecules. **(D)** Resolution estimate by FSC for the 3D reconstruction of the RS1 unit cell from micrographs of the 30° tilted specimen.

Table S1. **Primers used for cloning and introducing mutations into RS1**

Primer	Primer sequence
TOPO-RS1-F	5′-CGTTGCCCTTGTTTTTATGGTCGTATACATTTCTTACATCTATGCGGCCTCTACCGAGGATGAAGGCGAGGAC-3′
TOPO-RS1-R	5′-GGGGACAACTTTGTACAAGAAAGTTGGCTAATGGTGATGGTGATGGTGGGCACACTTGCTGACGCACTCCAGCAGC-3′
Adapter	5′-GGGGACAACTTTGTACAAAAAAGTTGGCACCATGAAATTCTTAGTCAACGTTGCCCTTGTTTTTATGGTC-3′
RS1-F	5′-GAGGCGGCCGCGCCACCATGTCACGCAAGATAGAAGGCTTTTTG-3′
RS1-R	5′-GCTCGAGTTAATGGTGATGGTGATGGTGGGCACACTTGCTGACGCACTC-3′
G91V-F	5′-GCAGTACGTGGTCTGGTATAGCT-3′
G91V-R	5′-TCTGGATTAGAACATGTGATCTG-3′
W92S-F	5′-GTACGTGGGCtcgTATAGCTCCT-3′
W92S-R	5′-TGCTCTGGATTAGAACATGTG-3′
Y93A-F	5′-CGTGGGCTGGtctAGCTCCTGGA-3′
Y93A-R	5′-TACTGCTCTGGATTAGAACATGTGATC-3′
R141H-F	5′-GACCCAGGGCcacTGTGACATCGATG-3′
R141H-R	5′-AGGATGCCGCTGATCACT-3′